Construction and Building Materials 397 (2023) 132341

Contents lists available at ScienceDirect

Construction and Building Materials

journal homepage: www.elsevier.com/locate/conbuildmat

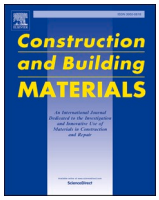

Electrochemical study on the chloride corrosion susceptibility of cementitious composites produced with sugarcane bagasse ash sand

Mariana de A.M. Rezende [a,b,c,*], Patricia G. Corradini [d,e], Almir Sales [a], Lucia H. Mascaro [d]

[a] Department of Civil Engineering, Federal University of São Carlos, Via Washington Luís, Km 235, São Carlos, SP 13565-905, Brazil
[b] Department of Science and Material Engineering, Federal University of São Carlos, Via Washington Luís, Km 235, São Carlos, SP 13565-905, Brazil
[c] Faculty of Exact Sciences and Technology, Pontifical Catholic University of São Paulo, Marquês de Paranaguá, 111, 01303-050, São Paulo, SP, Brazil
[d] Department of Chemistry, Federal University of São Carlos, Mailbox 676, CEP 13565-905, São Carlos, SP, Brazil
[e] Laboratório de Análises Químicas e Agroambientais, Fluminense Federal Institute of Education, Science and Technology, Campus Itaperuna, BR 356, Km 3, CEP 28300-000, Itaperuna, RJ, Brazil

ARTICLE INFO

Keywords:
Waste management
Concrete applications
Sugarcane bagasse ash sand
Chloride environment
Corrosion
Passivation
Aggregate

ABSTRACT

Sugarcane bagasse ash sand (SBAS) has been studied as a potential additive for reinforcement structures, but long-term (more than a week) studies on its use in test specimens have not been conducted considering the durability of these concretes. Additionally, there has been no assessment of electrochemical corrosion in corrosive media, such as chloride solutions. In this study, we conducted a physical and electrochemical investigation of SBAS, which partially replaces fine sand in a mortar configuration. Electrochemical impedance spectroscopy and open circuit potential monitoring techniques were used to evaluate the reinforcements in $Ca(OH)_2$ (curing environment) and NaCl 3.5% (aggressive environment), and SEM-EDS was used to analyze the reinforcement surface. During the curing process, SBAS concrete formed a passivation film after a longer time (7–14 days) than the reference (REF) (7 days), and the passive film showed higher resistance values than the REF sample. After 191 days in the chloride medium, REF and SBAS samples presented similar corrosion resistance. Therefore, SBAS-reinforced concrete could be a sustainable and effective alternative to conventional concrete for structural applications.

1. Introduction

Reinforcement corrosion is a major cause of degradation in reinforced concrete structures, significantly reducing their lifespan. This type of corrosion can cause a range of problems, including expansion, cracking, and chipping of the reinforced concrete cover, as well as structural damage due to the loss of adhesion between the steel bars and concrete.

Carbon steel can passivate in the pore solutions of Portland concrete, where the pH is around 13, resulting in the steel being in a passivated state according to the Pourbaix diagram for the iron-water system at 25 °C [1]. The pH range between 12 and 14 is generated by hydration reactions in the interstitial solution of concrete pores that produce hydroxides such as $Ca(OH)_2$, NaOH, and KOH. Within this range, steel behaves in a metastable manner and tends to oxidize, leading to the formation of solid compounds on the metal surface, due to the formation of a passive film [2]. However, although Pourbaix diagrams indicate whether the metal is in an immune, active, or passive corrosion stage based on the pH and potential of the metal, effective passivation is not always guaranteed. Several criteria must be met for effective passivation to occur. In addition to the stable oxides predicted by the Pourbaix diagram, these oxides must strongly adhere to the base metal and be densely and compactly, creating a thin but effective barrier that prevents accelerated corrosion of the bare metal.

Recycled additives, such as the by-products of sugarcane production have been studied as a potential solution to reduce the use of natural resources and waste. The ash from burning sugarcane bagasse can be found in the mills in two ways: light ash trapped in the chimneys, which is called sugarcane bagasse ash (SBA), and heavy ash collected at the bottom of the boilers, which is called sugar cane bagasse ash sand (SBAS), due to its quartz composition. These two types of sugarcane bagasse ash are not properly disposed of at the sugarcane plants, which means they are just piled up without use, even though they have the potential to be recycled.

* Corresponding author.
E-mail address: mamrezende@pucsp.br (M. de A.M. Rezende).

https://doi.org/10.1016/j.conbuildmat.2023.132341
Received 23 March 2023; Received in revised form 19 June 2023; Accepted 27 June 2023
Available online 11 July 2023

Table 1
Chemical composition of the sugarcane bagasse ash sand (SBAS) and ordinary Portland cement (OPC) used in this study.

Compounds	SiO_2	Fe_2O_3	K_2O	Al_2O_3	CaO	MgO	TiO_2	SO_3	CO_2	Na_2O
SBAS (wt.%)	91.30	3.00	0.50	2.30	0.40	0.20	0.90	–	–	–
OPC (wt.%)	19.17	3.21	0.61	5.03	65.73	0.61	–	2.84	2.38	0.52

Source: [7].

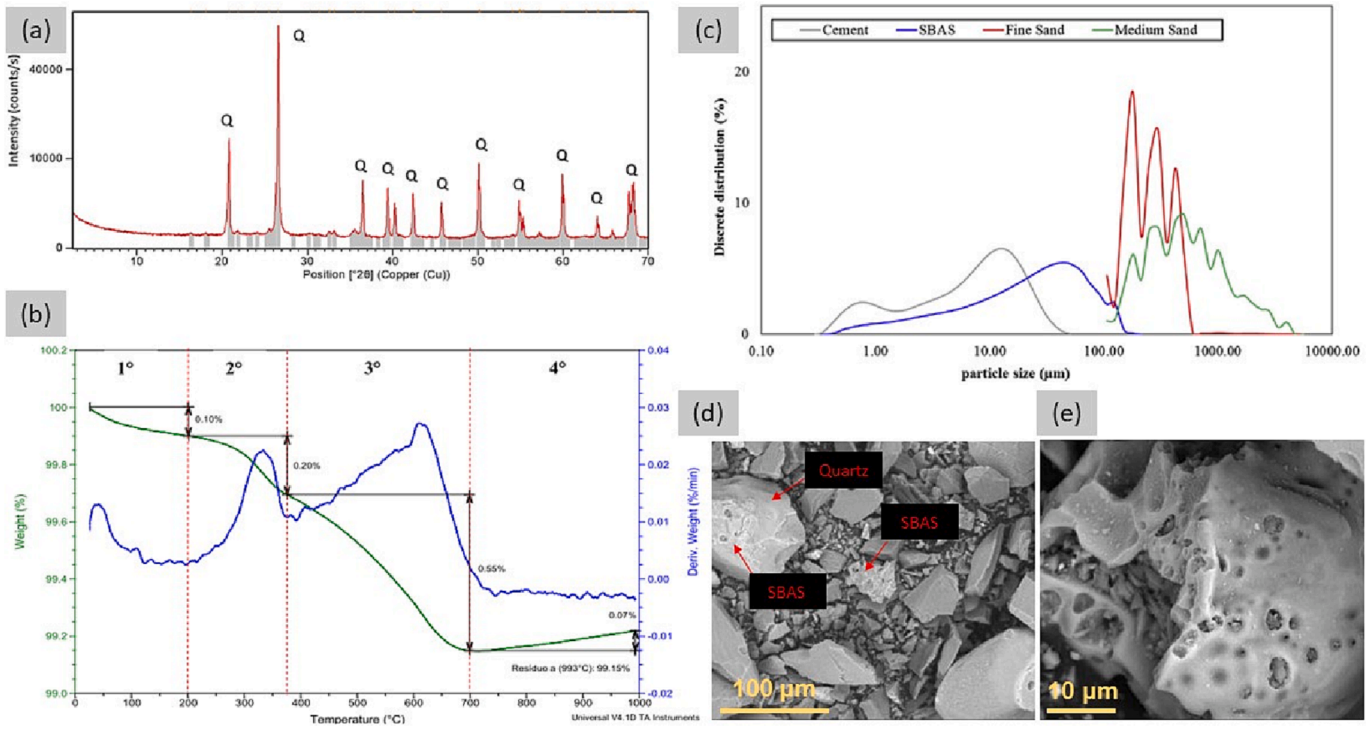

Fig. 1. Sugarcane bagasse ash sand characterization: (a) X-ray diffractogram of SBAS (Q = quartz) [7]; (b) SBAS thermogravimetry curves [21]; (c) Particle size distribution of cement, SBAS, fine sand, and medium sand [7]; and SEM-EDS of SBAS (d) particle on quartz; (e) smooth and porous surface SBAS particle [21].

Table 2
Chemical composition of AISI1005 used in this work.

Elements	Fe	C	Mn	P	S	Si	Cr	Ni	Mo	Cu
wt.%	99.098	0.054	0.384	0.027	0.036	0.081	0.077	0.059	0.014	0.170

Source: [28].

SBA has been used as a substitute for Portland cement in cementitious composites, and its proprieties have been analyzed since the mid-2000 s [3–5]. It has been demonstrated that using SBAS could increase the physical and mechanical properties of concrete and its durability [5,6] by reducing and changing the pore size distribution of the concrete [7]. Some authors have shown the possibility of using SBA as a partial replacement (5%, 10%, 15%, 20%, and 25%) for cement in concrete, considering mechanical properties, workability, water absorption, and other analyses. Their results indicated that a 5% replacement improved concrete strength and durability [8]. Another study analyzed the chemical behavior of SBA and the mechanical strength of cementitious composites with partial replacement of Portland cement with SBA. The cement paste results indicated a consumption of portlandite, showing pozzolanic potential [7]. The results also indicated the possibility of using a 15% substitution of Portland cement by SBA for mechanical strength [9]. Recently, other research has also been done using SBA as a pozzolanic material [10–13], observing that it saves on cement consumption and reduces CO_2 emission [14].

SBAS is normally used replacing this ash with fine aggregate, due to its high sand content in the composition, since it is a heavy ash. Sales & Lima (2010) [15] concluded that SBAS does not presented significant pozzolanicity, considered potentially inert. So, SBAS replaced natural sand by 10–100% in concretes for use in urban infrastructure artifacts. The authors pointed out that concretes produced with up to 30% SBAS can be used for the desired purpose. Other researchers used SBAS without processing as a partial substitute for natural sand in volume to produce concrete and the results of mechanical strength were satisfactory for the use of concrete for structural purposes [16]. Partially replacing fine sand, SBAS also was found to help increase the mechanical resistance and resistance to the drying-shrinkage strain for the concretes produced with SBAS, although increased the chloride ingress in this concretes [17]. However, these researches were carried out with ash *in natura* or just dried. The improvement in the properties of concretes and mortars with SBAS, however, is usually related to the filler and/or pozzolanic effect, which refine the pores of the concrete. Naturally, researches that were concerned with studying an efficient grinding of the SBAS reached better results regarding the increase of the physical and mechanical properties and the durability of concretes and mortars with this SBAS [6,7,18]. Regarding the corrosion of steel reinforcement, studies with simulated pore solutions have shown that incorporating

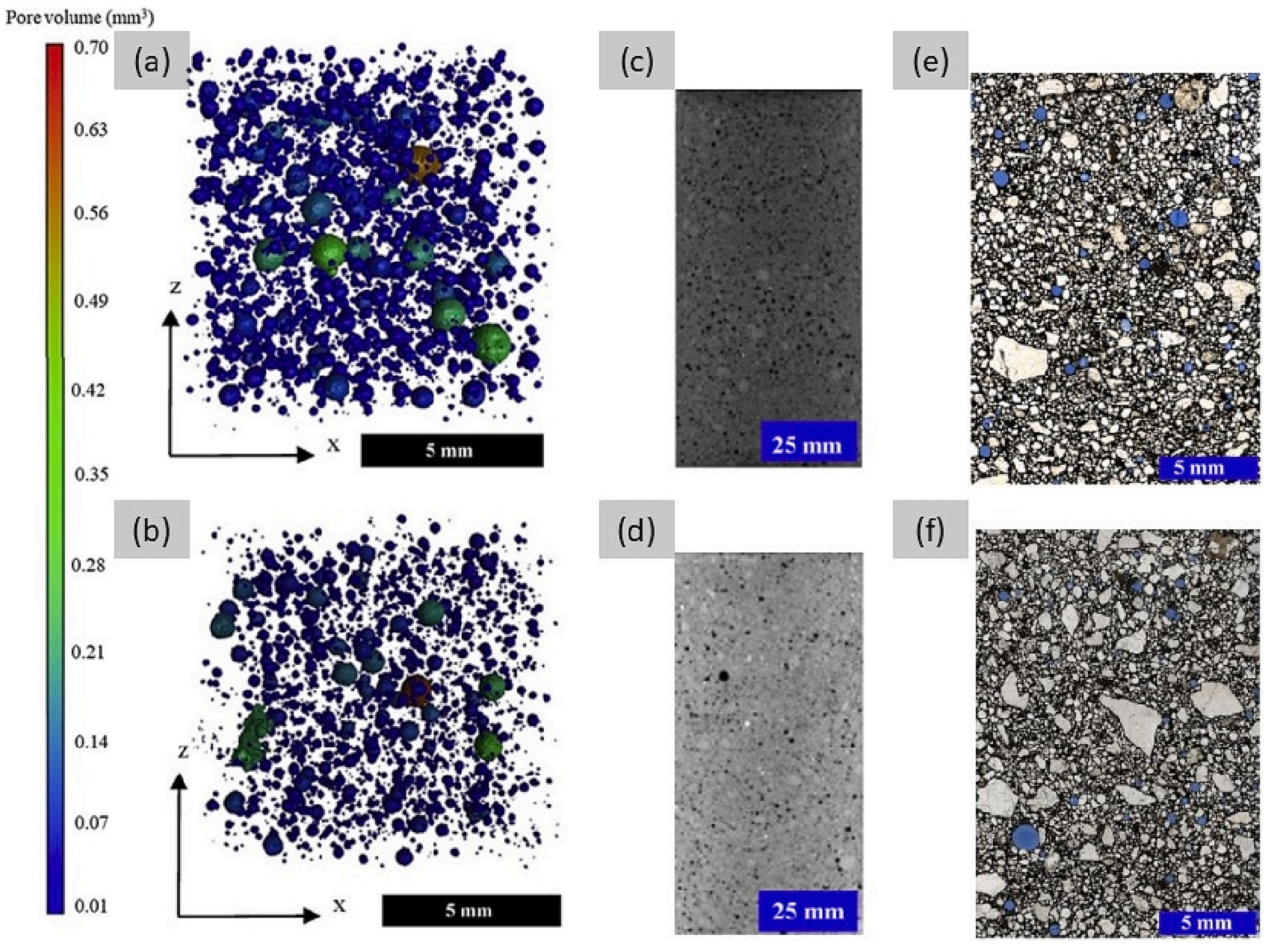

Fig. 2. X-ray computed tomography (CT) pore images of the (a) REF sample and (b) SBAS sample; CT images of cylindrical mortar (c) REF sample and (d) SBAS sample; Microscopic images of (e) REF sample and (f) SBAS sample [7].

Table 3
Mix proportions of materials used to produce the reference (REF) sample and the cementitious composite samples with partial replacement (30%) of sand with sugarcane bagasse ash sand (SBAS) and the flow diameters of the cementitious composites.

Group	SBAS content (%)	Mix proportion (by mass)					Flow diameter (mm)
		Cement	SBAS	Fine sand	Medium sand	w/c	
REF	0	1.000	0.000	1.350	1.650	0.55	256
SBAS	30	1.000	0.413	0.946	1.650	0.55	242

Source: [7].

Table 4
Physical properties and compressive strengths of the reference (REF) and mortars with a partial replacement (30%) of sugarcane bagasse ash sand (SBAS).

Group	Water absorption			Void ratio			Dry bulk density			Compressive strength (28 days)		
	Average value (%)	SD[a] (%)	CV[b] (%)	Average value (%)	SD[a] (%)	CV[b] (%)	Average value (g/cm³)	SD[a] (%)	CV[b] (%)	Average value (MPa)	SD[a] (%)	CV[b] (%)
REF	5.00	0.3	6	11.90	0.6	5	2374.30	16.40	1	45.75	1.0	2
SBAS	5.00	0.2	4	11.90	0.4	3	2358.40	10.80	0	49.68	1.7	3

[a]SD - Standard deviation.
[b]CV - Coefficient of variation.
Source: [7].

SBAS could function as a corrosion inhibitor [19]. The passivation film formed on steel in this medium showed better passivating properties. Therefore, SBAS seemed to be a potential recycled aggregate that could not only partially substitute for natural sand but also improve concrete durability. However, more than a week studies with this additive in test specimens, which would simulate the real application condition of this structure, have not been conducted. Additionally, there has been an assessment of electrochemical corrosion in corrosive media, such as chloride solutions.

Another major concern for civil construction is the finitude of natural

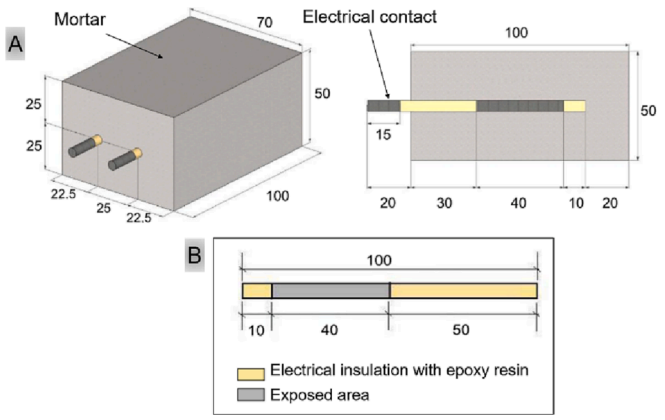

Fig. 3. Schematic representation of steel rebars in cementitious composite (A) and steel rebar delimitation areas (B), measured in mm.

resources that are important to produce concrete, such as natural aggregates (sand and gravel). The extraction process of sand and gravel cause decrease in the availability of these materials on the market and an increase in their price - for example, in the USA, the price of sand and gravel increased about 30 % from 2010 to 2020 [20]. Besides, natural sand sometimes must be transported from the extraction region to the region of use which means that its price can be even higher, the further from the extraction it is taken. Recycled sands, on the other hand, can be used conveniently in the origin region of the waste. Therefore, attempts to replace natural aggregates with recyclable ones are necessary.

Considering all that was mentioned, the main idea of this work is to evaluate SBAS as a corrosion inhibitor in reinforced concrete. As pore solutions may not realistically simulate the environment of steel behavior against corrosion in concrete, this work carried out experiments and analyses using test specimens of cementitious composites with SBAS. An electrochemical study on the durability of these cementitious composites was conducted by analyzing the passivation and corrosion of steel in the mortar with SBAS as partial sand replacement compared to a conventional reference mortar composite (REF). Two mediums of cementitious composites were evaluated: saturated $Ca(OH)_2$ solution to simulate the concrete curing process and NaCl solution to evaluate the resistance of concrete to chloride ions. The composites were physically and electrochemically characterized using electrochemical impedance spectroscopy (EIS), open-circuit potential (OCP), and scanning electron microscopy (SEM).

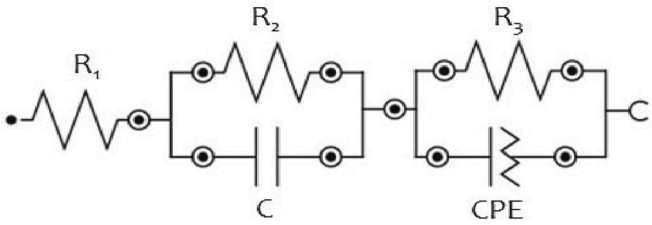

Fig. 5. The equivalent circuit used to fit the EIS data of rebars.

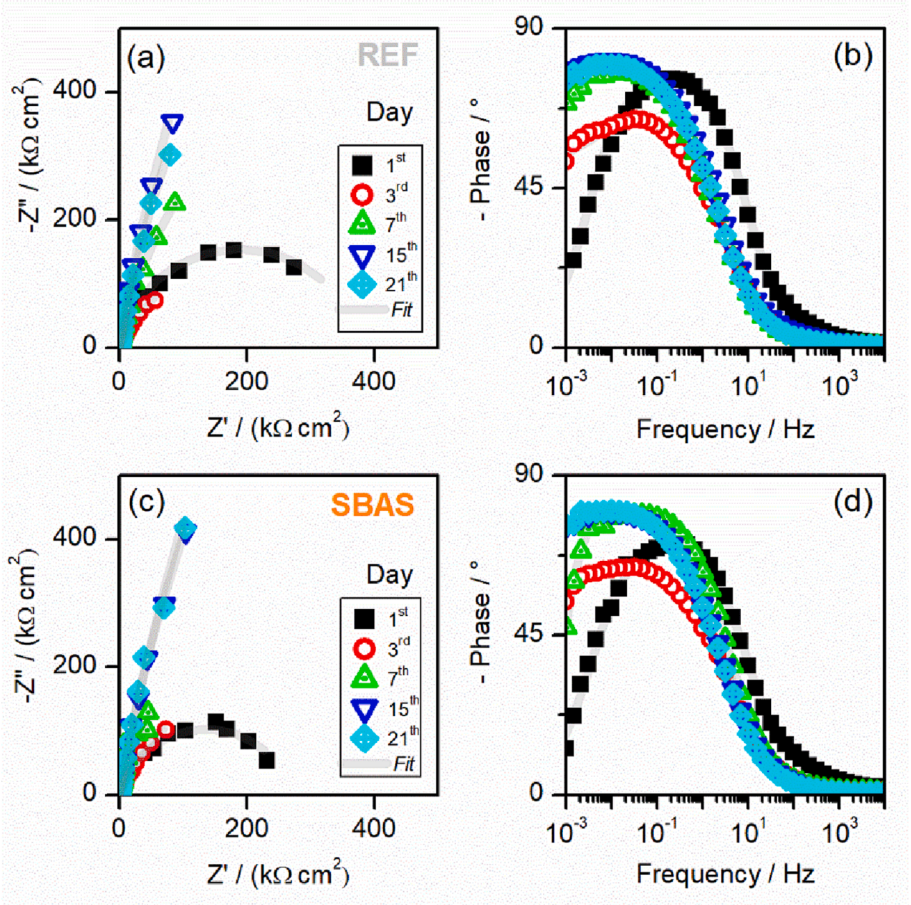

Fig. 4. Nyquist (a) and Bode (b) diagrams for steel in REF cementitious composites and Nyquist (c) and Bode (d) diagrams for steel in SBAS cementitious composites, all in $Ca(OH)_2$ solution. All measurements were made at 1, 3, 7, 15, and 21 days after the cementitious composites were molded.

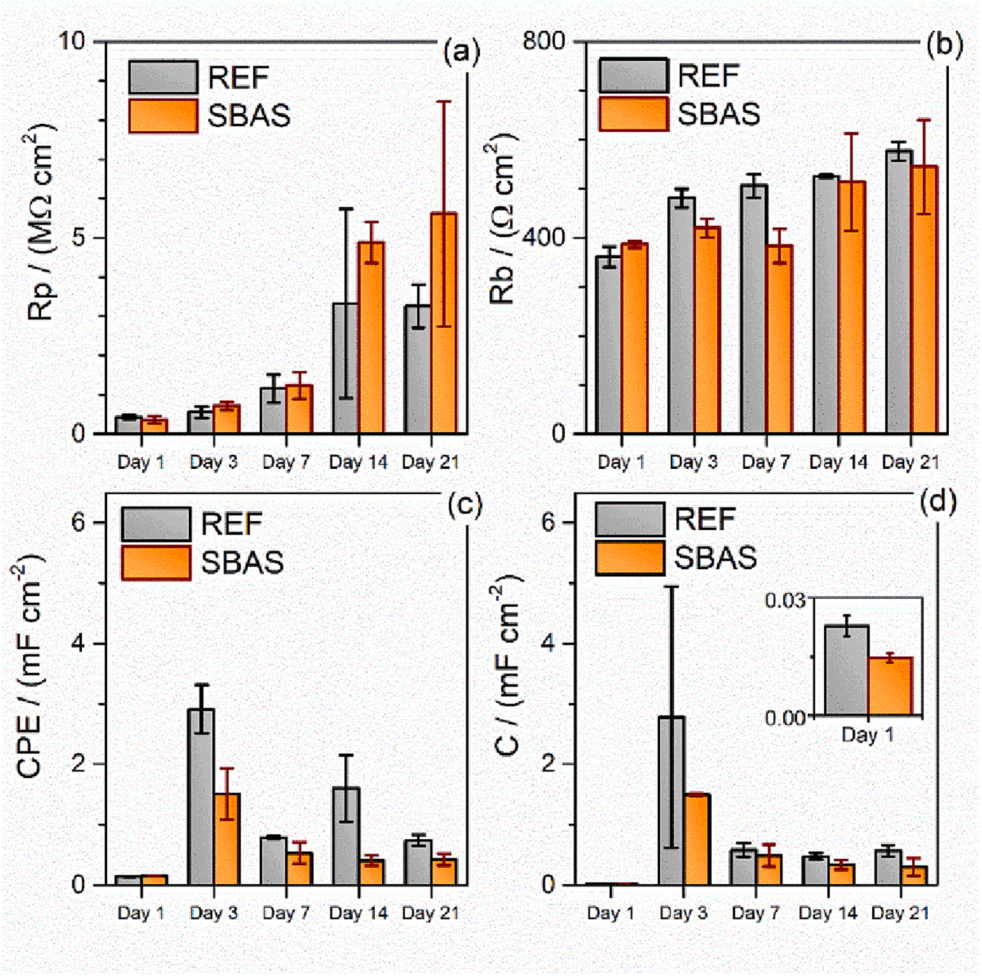

Fig. 6. (a) Polarization resistance (Rp), (b) cement matrix resistance (Rb), (c) constant phase element (CPE), and (d) capacitance (C) values obtained after fitting the equivalent circuit adopted as a function of the immersion time.

2. Material and methods

2.1. Materials characterization

Sugarcane bagasse ash sand (SBAS) is obtained from burning sugarcane biomass during the energy generation process at the factory, and the resulting ash is deposited at the bottom of the boilers, which is why it contains a considerable amount of sand and was named as sugarcane bagasse ash sand by the research group. The bottom ash from a sugarcane plant in the city of Jaú (southeast Brazil) was collected and taken to the laboratory. Sample preparation followed the experimental procedures in the literature, which involved subjecting the samples to a homogenization treatment by drying them at 100 ± 5 °C for 24 h, sieving them with a 2.4 mm square mesh, and grinding them in a ball mill for 240 min [7,18]. The resulting chemical composition (wt%) after this process shown in Table 1.

SBAS is a heavy ash that contain a large amount of sand in its composition, revealed by the chemical composition, in which SBAS samples showed high SiO_2 content (≥91.3%) and low loss on ignition (≤1.3%), as can be seen in Table 1. The X-ray diffraction test was carried out and characteristic peaks of quartz (Q) of high intensity were performed, thus showing quartz as the predominant mineral in the composition of SBAS. Characteristic but low-intensity peaks of hematite (H), cristobalite (C) and pseudobruchite (P) were also identified, as can be seen in Fig. 1(a).

The existence of well-defined peaks and the absence of an amorphous halo characterize the high degree of crystallinity of this material. In the quantitative analysis of the crystalline phases by the Rietveld method, it was identified that the SBAS samples are composed of 96% quartz. In addition to the quantitative analysis of the crystalline phases, the content of amorphous material existing in the SBAS was determined. The sample presented a content of 31.8% of amorphous material and 68.2% of crystalline material, leading to conclude that the SBAS is a predominantly crystalline material.

In the thermogravimetry test, four main transitions were observed, which are shown in Fig. 1(b). The first transition is associated with the loss of free water (temperature up to 100 °C). The second stretch of severe mass loss (between 200 °C and 375 °C) may be associated with the decomposition of organic compounds in the ash, such as hemicellulose, cellulose, and lignin [9]. The third stretch of mass loss is associated with quartz transformations. The most stable form of quartz at room temperature is alpha, and the change from alpha quartz to beta quartz occurs at a temperature of 573 °C, which is stable up to a temperature of 870 °C. From that point on, the transformation of beta quartz into tridymite occurs, and the transformation of tridymite into cristobalite occurs from 1470 °C and the melting point at 1713 °C [22]. In the last transition of the curve (from 700 °C) there was a mass gain, which may be associated with iron oxidation, corresponding to the transformation of magnetite into hematite [6]. These results corroborate the analysis by X-ray diffraction: the material is composed essentially of quartz, which is stable and shows practically no loss of mass when heated to 1000 °C.

The ash reactivity was verified by the following standard tests: modified Chapelle [23], pozzolanic activity index (PAI) with lime, and

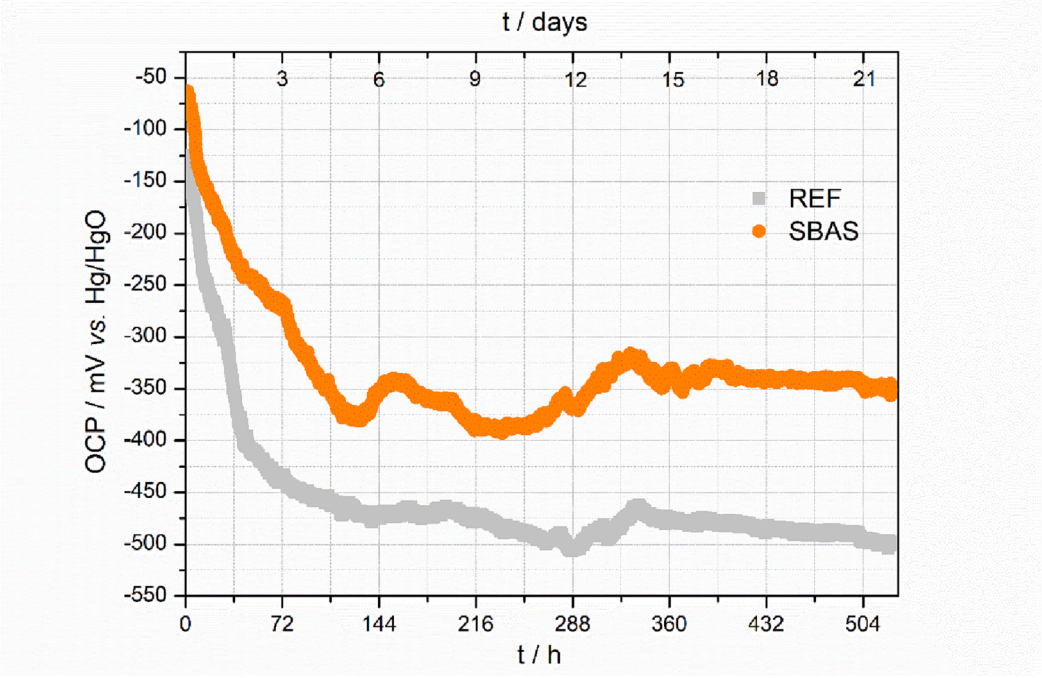

Fig. 7. The average of three open-circuit potentials (OCP) measured values as a function of the immersion time of the reference (REF) and sugarcane bagasse ash (SBAS) samples in a saturated $Ca(OH)_2$ solution.

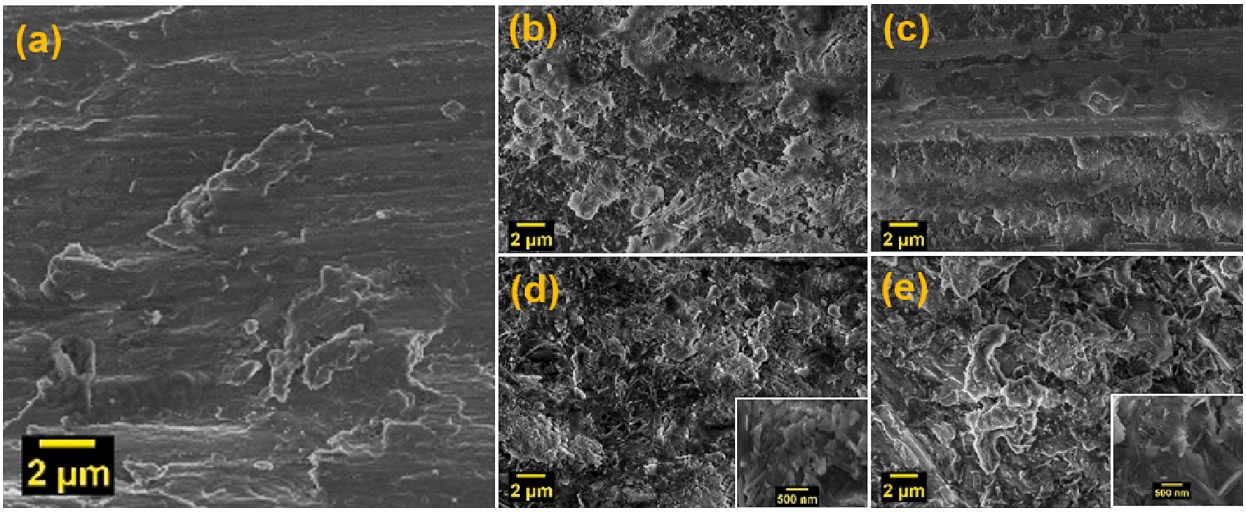

Fig. 8. SEM images of (a) steel as received; (b) REF 7th day; (c) SBAS 7th-day; (d) REF 21st day, and (e) SBAS 21st day.

PAI with Portland cement [24]. All SBAS samples showed low lime consumption. The result obtained was compared with the minimum lime consumption required for metakaolins, which should be 700 mg $Ca(OH)_2$/g of metakaolin. The lime consumption of SBAS samples corresponds to 22.1% of the minimum consumption required for metakaolins.

Despite the low lime consumption identified in the Chapelle test, it was possible to verify that the reduction in particle size led to an increase in the reactivity and/or filler effect of SBAS. The index of pozzolanic activity with lime was also below the necessary in all samples. The resistance was only 2 MPa, and this value corresponds to 1/3 of the necessary value (6 MPa) for the material to be considered as pozzolan, according to the specifications of NBR 12653 [25].

The SBAS samples also did not reach the minimum performance index with Portland cement, a value that corresponds to 90% of the resistance of the control mortar and did not present the minimum indexes necessary to be considered as pozzolanic materials.

After studying several grinding times for the SBAS, Moretti et al., [7] chose the sample where the granulometric distribution fit between fine sand and cement, with the aim of filling the existing granulometric gap (240 min of griding) Also, Fig. 1(c) displays the particle size distribution of the other materials used, which was determined using a laser particle size analyzer for OPC and SBAS and a test sieve shaker for fine and medium sand (E323 [26]). The specific gravity values were found to be 2.69 g cm^{-3} for the SBAS material, 2.64 g cm^{-3} for fine sand, and 2.60 g cm^{-3} for medium sand.

SBAS samples were also analyzed by scanning electron microscopy (SEM) with EDS analysis. Fig. 1(d) shows the presence of quartz and ash particles in SBAS and Fig. 1(e) shows the smooth and porous surface of a SBAS particle.

Considering all the characteristics analyzed on the SBAS, in this work and in other works of the research group, it was chosen to be used as fine recycled aggregate. In addition to the similarities of SBAS with fine

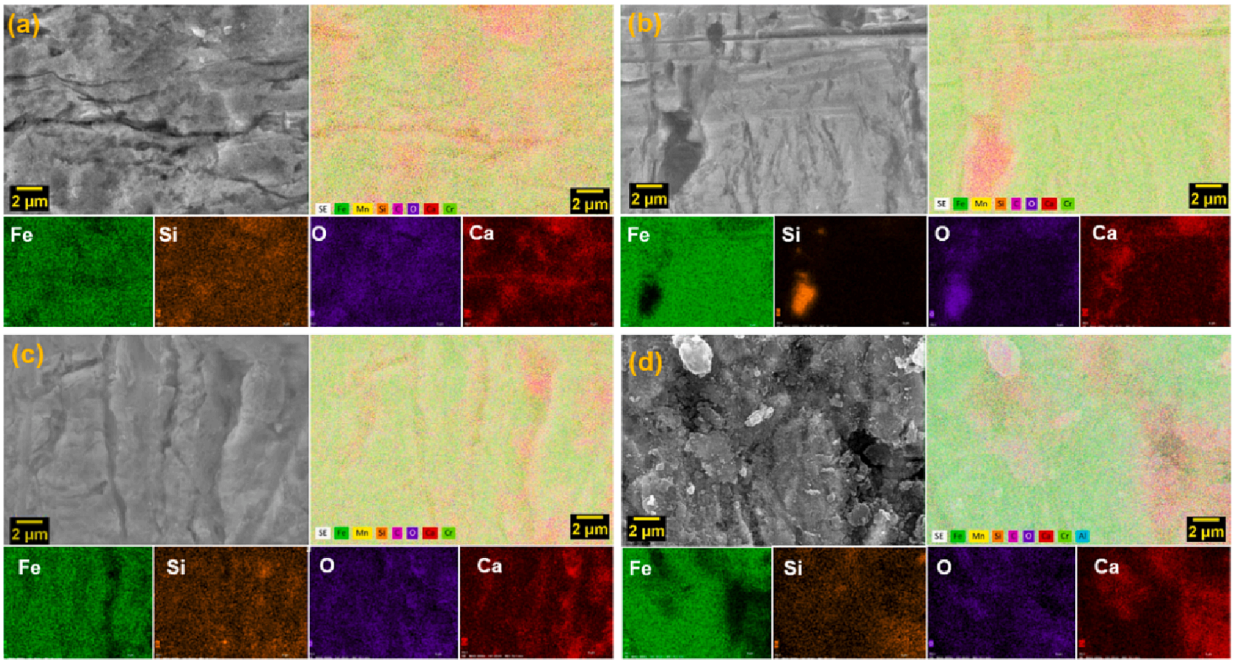

Fig. 9. SEM with elemental mapping (Fe, Si, O, Ca) of (a) REF 7 days, (b) SBAS 7 days, (c) REF 14 days, and (d) SBAS 14 days in $Ca(OH)_2$ saturated solution.

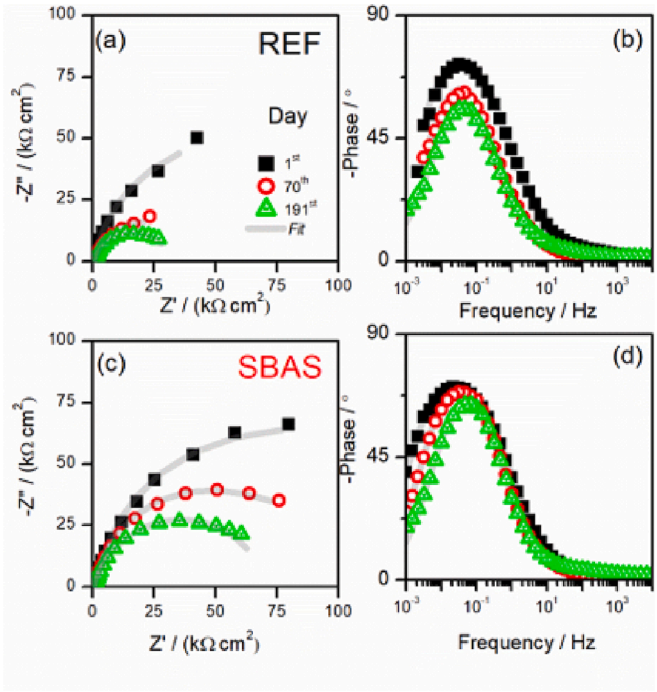

Fig. 10. Nyquist (a) and Bode (b) diagrams for REF mortar and Nyquist (c) and Bode (d) diagrams for SBAS mortar in NaCl 3.5% solution. All measurements were made at 1, 70, and 191 days of solution exposure.

aggregate and its low pozzolanicity, as mentioned in item 1, the objective of this work was also to find alternatives for recycled aggregates, since natural sand is increasingly scarce in the world.

The other materials used in this study were Portland cement with high early strength and a 3.79% loss on ignition (Table 1) and quartz fine and medium sand, both obtained from the São Carlos City area (São Paulo, Brazil).

As the working electrode, for the passivation and corrosion tests, 5 mm diameter AISI 1005 steel, typically used in civil construction in Brazil was cut into 100 mm bars. The steel samples were cleaned following ASTM G1-03 [27]. Hg/HgO/KOH (1 mol/L) was employed as the reference electrode (RE) for the passivation analysis, and a saturated calomel electrode (SCE) was employed as the RE for the corrosion analysis. A titanium cylinder was used as the auxiliary electrode (AE). The chemical composition of AISI1005 was determined by atomic absorption spectroscopy (Inductar CS cube analyzer) shown in Table 2.

After choosing and characterizing the materials, mortar samples were molded.

2.2. Mortars characterization

As the objective of this work was to analyze the passivation and corrosion of carbon steel in porous cementitious media, mortar samples were molded with embedded steel. Mortars samples were molded with SBAS (denoted as SBAS) and without SBAS (denoted as REF) as the reference.

The literature indicates that replacing 30% of natural sand (in volume) with SBAS is the optimal proportion for improving the physical, mechanical, and durability properties of concrete with the aim of using the maximum amount of SBAS that does not harm the properties of concrete with this residue [6,7].

Moretti et al., [7] studied SBAS mortars with 10%, 20%, 30% and 40% of sand replacement by SBAS. In their research, with X-ray computed tomography (Fig. 2) it was concluded that the presence of SBAS: 1) changed the pore size distribution but did not affect the porosity of the mortars; 2) produced mortars with lower volume of macropores comparing to the REF mortar. Specially, mortars with 30% SBAS presented a reduction of 44% of macropores larger than 0.1 µm. Therefore, 30% SBAS replacement by natural sand in mortar have the potential to improve durability. This improvement was confirmed by the lower carbonation depth of 30% SBAS mortars [6] and higher polarization resistance of passivation film formed on the steel of this mortar in 30% SBAS aqueous media [19].

Considering all the benefits to substitute natural sand by SBAS in the proportion of 30%, in this research, this replacement was used to understand the behavior of carbon steel immersed in mortars with 30% SBAS.

The mixture proportions of the materials used to produce the

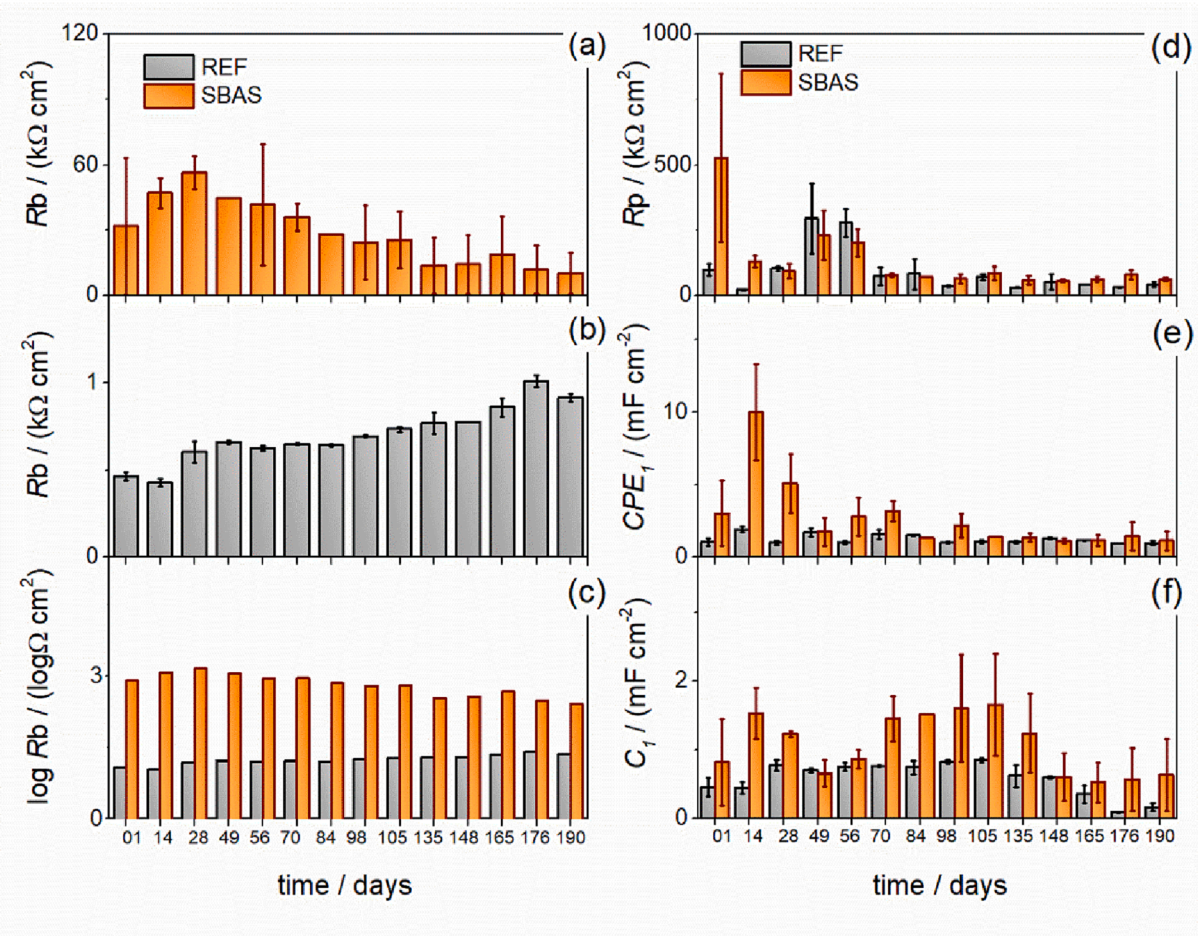

Fig. 11. Evolution of concrete resistance with the age of the (a) reference sample, (b) SBAS sample, (c) logarithm of the concrete resistance, (d) polarization resistance, (e) constant phase element (CPE) and (f) capacitance (C) values of REF and SBAS samples obtained by fitting the equivalent circuit in Fig. 4 as a function of the immersion time in 3.5% NaCl solution.

cementitious composites as well as the flow diameters determined according to Brazilian standard NBR 13276 [29], are shown in Table 3.

Table 4 summarizes the results of the physical properties and compressive strengths of REF and SBAS samples obtained from previously published research [6]. Water absorption, void ratio, and dry bulk density values did not present a significant difference when comparing SBAS to REF samples [30]. Moreover, the compressive strengths for REF and SBAS are statistically equivalent, considering a significance level of 5% (ANOVA). Therefore, considering the properties mentioned, there was no problem with using SBAS as a partial replacement of sand in structurally reinforced concrete.

2.3. Test samples

The size of the cementitious composite samples was 70 × 50 × 100 mm (Fig. 3A). Fig. 3B shows a schematic representation of the steel rebars' electrical insulation. The exposed electrode area was 6.28 cm2 (Fig. 3B), which was considered in the electrochemical impedance spectroscopy measures. For each electrochemical measurement, two REF and two SBAS samples were molded, so four carbon steel samples were monitored.

These materials and samples of cementitious composites were used to carry out the electrochemical characterization in this work.

2.4. Electrochemical characterization

All the electrochemical characterizations were performed in a conventional three-electrode glass cell at 23 °C using an Autolab-PGSTAT20 potentiostat/galvanostat equipped with a FRA32 module.

The open-circuit potential (OCP) was monitored for 222 consecutive days (28 days in $Ca(OH)_2$ saturated solution and 191 days in 3.5% NaCl solution). Electrochemical impedance spectroscopy (EIS) was performed at the OCP in the 10 kHz to 1 mHz frequency range, applying a 10 mV AC modulation. Frequency sampling was 6 points per decade. All the EIS spectra were curve-fitted using Nova 2.1.4 software.

The *ex-situ* characteristics of the working electrode surface on the different cementitious composite samples were also conducted at different periods of immersion in saturated $Ca(OH)_2$ solution and 3.5% NaCl solution. The morphology and elemental composition of the passive films formed and the corrosion products were investigated using SEM with high-resolution field emission using an FEG-SEM ZEISS SUPRA 35, coupled to energy dispersive spectrometry.

3. Results and discussion

3.1. Cementitious composite monitoring in alkaline medium

EIS measurements were performed on this system to obtain information about surface films, concrete characteristics, interfacial corrosion, and mass transfer phenomena [31]. Fig. 4a and b show the Nyquist and Bode diagrams for the REF cementitious composite, respectively. Fig. 4c and d pertain to the SBAS cementitious composite, all in a saturated $Ca(OH)_2$ solution. The Nyquist diagrams indicated that on the first day, both the REF and SBAS samples formed a semicircle, and the

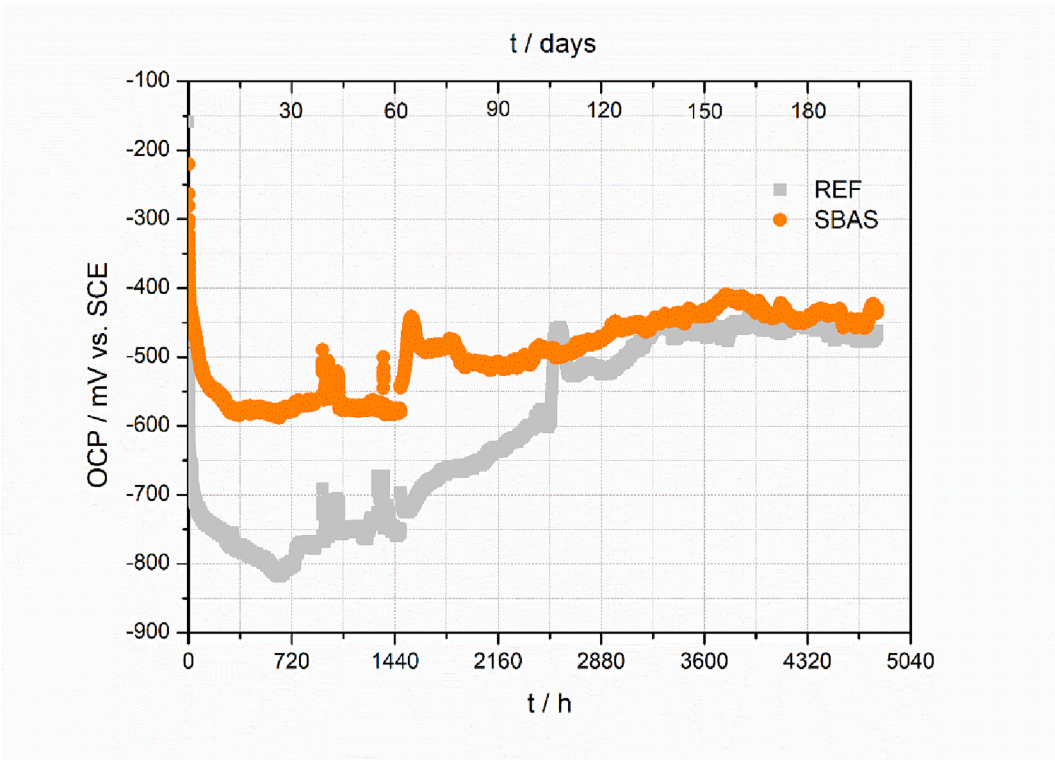

Fig. 12. Evolution of the average of three open-circuit potentials (OCP) measured values as a function of immersion time of reference (REF) and sugarcane bagasse ash (SBAS) samples in 3.5% NaCl solution.

smaller the semicircle, the higher the susceptibility to corrosion [31]. Increasing the exposure time to $Ca(OH)_2$ solution resulted in an expansion of the semicircle. As this solution is alkaline and the potential range of carbon steel in concrete is taken into account, as per the Pourbaix diagram [32], a passivation process probably occurred in the steel, especially between the 3rd and the 7th day for both REF and SBAS samples.

To better understand the electrochemical interfaces of the system, the spectra were modeled by an equivalent circuit model (Fig. 5) to fit the observed phenomena. The low-frequency points on the Nyquist plot (10^{-3} Hz to 10 Hz) correspond to the resistance of the electrode (R_3). They are associated with the concrete interface with the steel rebar, where the corrosion phenomenon occurs. The smaller the radius of this semicircle, the higher the susceptibility to corrosion. The phenomena that occur at medium frequencies (10^2 Hz to 10^6 Hz) correspond to the concrete resistance (R_2) and are associated with the characteristics of the cementitious matrix that surrounds and protects the reinforcement. At high frequencies ($>10^6$ Hz), there is an offset resistance (R_1) that is not of much interest to the process and is without any apparent physical significance. In practical terms, R_1 can be neglected, and the cement matrix resistance (R_b) can be estimated as $R_b = R_1 + R_2$ [6,27,29,30]. In this case, the capacitance related to the cement matrix behaves like an ideal capacitor (C), but the one related to the reinforcement is like a non-ideal capacitor, so a constant phase element (CPE) was adopted.

Fig. 6 shows the parameter values obtained after fitting the equivalent circuit with EIS data. The presented values refer to the average for both rebars in one cementitious composite sample. The electric double-layer resistance (Rp) results were consistent with the formation of a passivating film, which increased over time (Fig. 6a). The concrete resistance ($Rb = R_1 + R_2$) for both the reference and SBAS samples remained practically constant and had the same values after the 7th day, considering the associated error (Fig. 6b). This parameter is crucial in EIS analysis because it quantitatively shows the resistance to electron transfer for the system, for example, the corrosion resistance. Additionally, the average value of Rp in SBAS samples was higher than in REF samples after 14 days of the curing process, providing additional evidence that the passivating film formed on steel in an SBAS environment is more protective than that formed on steel in a conventional cementitious matrix. After the 3rd day, both REF and SBAS samples exhibited decreasing CPE and C values over time (Fig. 6c and Fig. 6d), indicating a more oxidized surface due to the formation of a passive oxide film [34]. The SBAS sample is also less capacitive than the REF sample. For better visualization, Figure S1, available in the Supporting Information (SI), presents a simulated Nyquist plot for the average responses for REF and SBAS cementitious composites (Fig. 6). The semicircle effect increased with exposure time for both conditions. In the SBAS medium (Fig. S1a), the resistance value is higher than in REF (Fig. S1b) for the same period. Since concrete is a highly resistive and heterogeneous composite, some of the estimated EIS parameters have a high associated error. Some authors have noted difficulties in analyzing EIS data in this situation [26,27], but this technique is widely used for assessing corrosive processes in concrete.

The OCP was monitored at regular intervals for 22 days while the cementitious composite samples were immersed in a saturated $Ca(OH)_2$ solution. The averages of three measurements performed on the REF and SBAS samples are shown in Fig. 7. The OCP of REF began near −125 mV and showed a decrease of -2.5 mV h^{-1} for the first 138 h. From 120 h to 504 h, it showed a small -0.08 mV h^{-1} variation until the end of the measurement, with a value of −497 mV (-662 mV *vs.* reversible hydrogen electrode - RHE). The OCP measured in the SBAS samples also showed a great decrease in the beginning, with a 2.5 mV h^{-1} rate in the first 127 h. From 127 h to 409 h, it showed an average growth of 0.14 mV h^{-1} before stabilizing at around −345 mV (-510 mV *vs.* RHE). The decrease in OCP in an alkaline solution is related to the difficult mass transport of oxygen at the cementitious matrix/steel interface [6,28]. Similar behavior has been observed by other researchers who have linked the decreasing OCP to a reduction in current density [6,28–30]. When the OCP of a system comes into equilibrium, it indicates that the

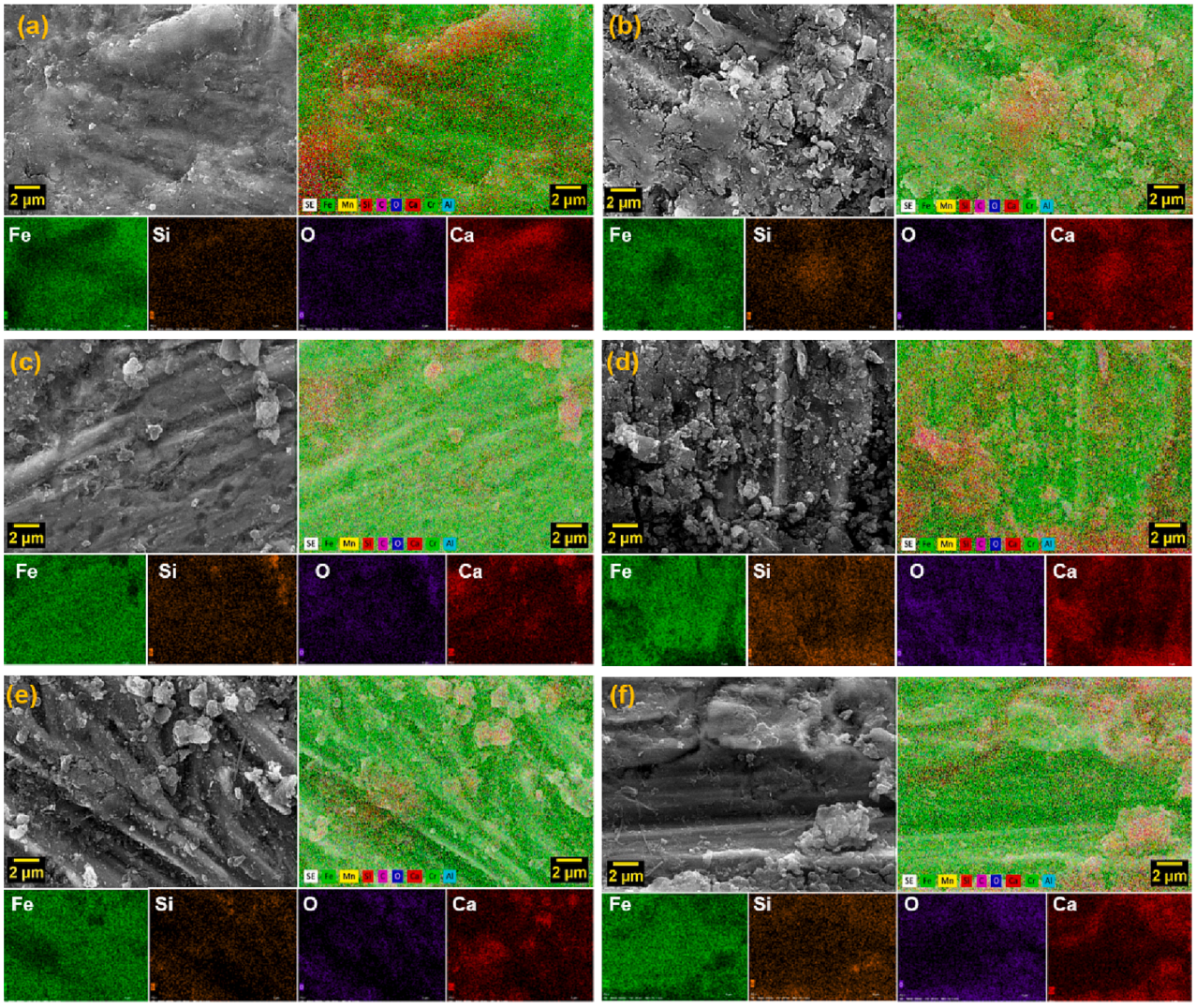

Fig. 13. SEM with elemental mapping (Fe, Si, O, Ca) of (a) REF 14 days, (b) SBAS 14 days, (c) REF 60 days, (d) SBAS 60 days, (e) REF 191 days, and (f) SBAS 191 days in 3.5% NaCl solution.

surface is less susceptible to the corrosion process. Therefore, it suggests that REF is in a passivation stage after 144 h (6 days) and SBAS after 360 h (14 days), considering the 11.67 pH measured in the solution and the Pourbaix diagram [32].

Scanning electron microscopy (SEM) images of the as-received steel sample (blank sample), the reference sample, and the sample with SBAS at 7 and 21 days can be seen in Fig. 8. The blank sample (Fig. 8a) showed only scratches due to the steel cleaning process. A coating structure was observed on the 7th-day reference sample (Fig. 8b), which is likely the passivating film formation as indicated by EIS and OCP measurements. Structures similar to ettringite were also observed, which is described in the literature by the cementitious composite age [35]. In the 7th-day SBAS samples (Fig. 8c), the coating on the steel was less distributed than in the REF sample. Based on OCP and EIS analysis, the complete formation of the passivating film for SBAS samples was observed at approximately 14 days (see Fig. 6a and b). On the 21st day, the passivating film on the REF sample (Fig. 8d) had covered the steel, and there was no formation of ettringite at this age. However, on the 21st day for SBAS, a steel overlay structure was formed. Based on the OCP and EIS results, these structures, in the presence of SBAS, result in a more protective layer than that formed in the REF cementitious composite.

SEM images with elemental mapping (Fe, Si, O, Ca) of the steel surface after 7 and 14 days in REF and SBAS samples were obtained (Fig. 9). On the 7th day of immersion in a saturated $Ca(OH)_2$ solution, the REF sample (Fig. 9a) showed a surface covered with the four elements analyzed: Fe from the steel, Si, from the cementitious matrix, and O and Ca from the solution. Since iron and oxygen are uniformly distributed on the steel surface, it is possible to associate them with passive film formation. In the SBAS sample immersed for 7 days in the same solution (Fig. 9b), the iron was distributed on the surface, but the oxygen was not, which is an indication that the passivating film was not fully formed in these samples. Additionally, an area in the lower-left corner of the image was observed, mainly composed of Si, possibly a cementitious composite inlay on the steel sample. In Fig. 9c and Fig. 9d, corresponding respectively to REF and SBAS immersed for 14 days in saturated $Ca(OH)_2$ solution, Fe and O are uniformly distributed on the steel surface, indicating the formation of a passive film on the surface, along with the other analyses performed. Therefore, this analysis also corroborates what has been exposed previously. At 7 days, the passive film was already well-formed in steel on REF, and for SBAS, the passive film is formed at the end of the 14th day. The later formation of the protective film in the SBAS medium is not a problem since, for practical purposes, the curing time of the conventional reinforced concrete structure is normally 28 days, and the concrete shoring structure can only start being removed after 14 days [36].

The weight percentage of carbon, oxygen, silicon, calcium, and iron

in the REF and SBAS samples at 7 and 14 days of immersion in a saturated $Ca(OH)_2$ solution are presented in Figure S2 in SI. The percentage of C, O, Si, and Ca in the REF samples decreased from 7 to 14 days of immersion, whereas the percentage of Fe showed a small increase. In contrast, the SBAS samples showed an increasing percentage of C, O, and Ca from 7 to 14 days of immersion, while the amount of Si remained almost constant, and the amount of Fe decreased. The percentage of passivating film-forming products in steel (O and Fe) was expected to increase between 7 and 14 days, along with the C, forming the steel, decreasing since the surface of the steel would be covered by the passivating film according to the analyses carried out. However, this did not happen due to difficulties in cleaning the steel sample that was removed from the cementitious composite sample without damaging the passivating film. Therefore, dirt was observed in the steel sample, probably due to the presence of cementitious composite remains that could not be seen with the naked eye.

In summary, at 7 days of immersion, this work hypothesizes that the steel sample from REF presents a formed passivation film, while the steel sample from SBAS presents film formation between 7 and 14 days of immersion in the solution. However, the passivating film formed on steel in the SBAS environment seems to be more protective than steel in a conventional cementitious environment. Our group [19] also reached the same conclusion while analyzing the same steel in concrete pore solution with SBAS, although the passivation film formed on the steel in the SBAS medium took 3 days and in the medium without SBAS, it took 2 days, due to higher ionic mobility in the solution compared to the cementitious composite.

3.2. Cementitious composite monitoring in chloride medium

After the REF and SBAS samples were immersed for 28 days in saturated $Ca(OH)_2$ solution (curing time of conventional concrete), they were fully immersed in 3.5% NaCl solution, simulating the seawater, as recommended by the ASTM standard C876 [37]. In contrast to the standard method, the samples in this study were regularly monitored for 200 days using EIS and OCP.

EIS measurements for samples in 3.5% NaCl solution were performed using the same measurement parameters as saturated $Ca(OH)_2$ solution, and the same equivalent circuit was used to fit the data (Fig. 5) because the physical phenomenon is the same. Fig. 9a and b show the Nyquist and Bode diagrams for the REF cementitious composite, respectively, and Fig. 10c and 10d are for the SBAS cementitious composite. Although EIS measurements were performed every seven days, only the data from the 1st, 70th, and 191st days are shown in Fig. 10 to facilitate visualization of the corrosion evolution in the samples. The Nyquist plots show a decrease in the capacitive loop diameter with time in both the SBAS and REF samples, indicating that the corrosion in steel increases during the time of exposure to the chloride solution. Comparing the impedance spectra of the REF (Fig. 10a) and SBAS (Fig. 10c) samples, the SBAS sample has a larger diameter at low frequencies, which means that it has a greater polarization resistance compared to the REF sample. From the Bode diagrams for REF (Fig. 10b) and SBAS (Fig. 10d), the phase angle for REF samples decreased more over time than the phase angle of the SBAS sample, also showing that the steel sample in SBAS is more protected from corrosion.

Fig. 11 presents the EIS parameters obtained from data fitting. Fig. 11a and b show the concrete resistance (R_b) over time for the REF and SBAS samples, respectively, while Fig. 10c presents the Rb values in the logarithmic scale for comparison. The R_b of the cementitious composite with SBAS is up to 6 times higher than that of the reference concrete. The polarization resistance (R_p) measurements of the REF and SBAS (Fig. 11d) decreased over the exposure time in the aggressive solution. The capacitances related to the corrosive process (CPE) and concrete (C) are shown in Fig. 11e and 11f, respectively. The CPE increased from the first to the 14th day and then only decreased over the time of immersion in NaCl solution for both samples. The C values for the REF sample were constant until the 148th day and then showed a drop. For SBAS, the value showed an oscillation with small increases until the 14th day, followed by a C value decreasing until the 49th day, after which the behavior repeated the increasing/decreasing process. Despite this variation, C and CPE values for SBAS were higher than for REF, especially for the first 90 days. This effect may be related to the chloride permeability and diffusion into the concrete, which depends on the porosity, pore diameters, and air content of the concrete [23,33]. The electrical conduction is correlated not only to the pore structure characteristics but also to the electrical conductivity of the pore solution [38]. A study showed that chloride permeability for bagasse ash-blended concrete is considerably reduced by a partial replacement of high-strength Portland cement with bagasse ash sand [38]. However, the permeability of the concrete was measured for 191 days exposures of the concrete, and the values of R_p, CPE, and C are similar for the concrete with and without the addition of SBAS. A highlight point is that the SBAS addition does not damage the corrosion resistance of the reinforcement, enabling the use of this material for construction.

Fig. 12 shows the average of three measurements performed on REF and SBAS samples in 3.5% NaCl solution. For SBAS, the OCP started near −200 mV (*vs*. SCE). However, within two weeks, the OCP decreased rapidly at a rate of approximately −41 mV day^{-1}, stabilizing at around −575 mV for 45 days. Subsequently, the potential increased at a rate of 15 mV day^{-1}, reaching approximately −500 mV. From the 105th day, the OCP had a small increase of around 0.41 mV day^{-1}, stabilizing at 30 days near −440 mV for the SBAS sample. On the other hand, for the REF sample, the OCP started at a similar value as the SBAS sample but decreased rapidly at a rate of about −360 mV day^{-1} until the second day, when the potential was −715 mV (*vs*. SCE). Then, the OCP decreased at a rate of −4 mV day^{-1} and remained at −810 mV on the 26th day. Between the 26th and 135th day, the OCP increased to −470 mV and stayed at this value until the end of the experiment. At 191 days, the OCP values of the REF samples (-711 mV *vs*. RHE) and SBAS samples (-681 mV *vs*. RHE) were similar. Based on a solution pH of 9.98 and the Pourbaix diagram [32], the steel was in the immunity/passivation interface region. However, according to the EIS measure and some studies, the steel is in an active corrosion region at the end of 191 days in a 3.5% NaCl solution [10,24]. Moreover, the oscillations and fluctuations in OCP values could be attributed to localized corrosion/passivation processes, typical of chloride media at low oxygen diffusion in the concrete [10].

Fig. 13 shows SEM images and elemental mapping obtained from REF and SBAS samples at 14, 60, and 191 days of immersion in 3.5% NaCl solution. Fig. 13a and b show REF and SBAS images taken after 14 days of immersion, respectively. Iron and calcium are well distributed in both samples, but more iron is observed on the surface of SBAS. Analysis of the weight percentage of the most abundant elements found on the steel samples (shown in Figure S3 in the SI) reveals a similar quantity of carbon, calcium, and iron in REF and SBAS after 14 days of immersion. Oxygen and silicon are present in lower quantities in REF compared to SBAS. The presence of Ca and Si is attributed to a cementitious composite residue that was not visible during sample preparation. After 60 days of immersion, REF showed an increase in the amount of C and Fe and a decrease in the amount of O and Ca. Si remained practically constant.

Analyzing the SEM images, it appears that the layer better covers the SBAS samples than the REF samples, suggesting that the corrosion products may be more spread out in the former due to the higher amount of oxygen present. The samples exposed to the action of chlorides for 191 days visually presented a similar surface to those exposed for 60 days for the two samples analyzed. However, the weight percentage of the elements showed that SBAS samples have a greater amount of oxygen than REF samples, indicating a more protective passive film. These findings confirm that the SBAS environment is more protective for steel.

4. Conclusions

In this study, a physical and electrochemical investigation was conducted with SBAS, which partially replaced fine sand in a mortar configuration. In an alkaline environment, the reinforcement of REF and SBAS concrete formed a passivation film around 7 days and 7–14 days, respectively. However, SBAS exhibited a more protective film than conventional cementitious environments, as demonstrated by EIS parameters and SEM-EDS analyses.

Furthermore, after seven months of exposure to a chloride medium corrosion behavior shown to be similar for concrete with and without SBAS. The values of Rp, CPE, and C were comparable, indicating that steel in both environments, the steel underwent a similar corrosion process.

Overall, these findings suggest that the use of SBAS in cementitious composites is a promising approach not only for disposing of agro-industrial waste but also for maintaining or even enhancing the corrosion resistance of the reinforcement. Therefore, SBAS-reinforced concrete could be a sustainable and effective alternative to conventional concrete for structural applications.

CRediT authorship contribution statement

Mariana de A. M. Rezende: Investigation, Methodology, Data Curation, Writing – Original draft preparation. **Patricia G. Corradini:** Investigation, Methodology, Data Curation, Writing – Original draft preparation. **Almir Sales:** Conceptualization, Supervision, Writing – Reviewing and Editing, Project administration, Resources. **Lucia H. Mascaro:** Visualization, Supervision, Writing – Reviewing and Editing Resources.

Declaration of Competing Interest

The authors declare that they have no known competing financial interests or personal relationships that could have appeared to influence the work reported in this paper.

Data availability

The raw/processed data required to reproduce these findings will be made available on request.

Acknowledgments

The authors thank the Instituto de Pesquisas Tecnológicas (IPT) for the steel chemical analyses and the Laboratory of Structural Characterization (LCE/ DEMa/ UFSCar) for the general facilities. Also, the authors thank the Sao Paulo Research Foundation (FAPESP) for the grant received [#2013/07296-2, #2018/16401-8], along with Coordenação de Aperfeiçoamento de Pessoal de Nível Superior (CAPES) [Finance Code #001] and National Council for Scientific and Technological Development – CNPq for their financial support [grants #303407/2020-4, #307230/2018-0 and #151572/2022-4].

Appendix A. Supplementary data

Supplementary data to this article can be found online at https://doi.org/10.1016/j.conbuildmat.2023.132341.

References

[1] B. Beverskog, Revised diagrams for iron At 25–300 ° C, Science 38 (1996) 2121–2135. http://www.sciencedirect.com/science/article/pii/S0010938X96000674.
[2] W.K. Green, Steel reinforcement corrosion in concrete–an overview of some fundamentals, Corros. Eng. Sci. Technol. 55 (2020) 289–302, https://doi.org/10.1080/1478422X.2020.1746039.
[3] G.C. Cordeiro, R.D.T. Filho, E.M.R. Fairbairn, L.M.M. Tavares, C.H. Oliveira, Influence of mechanical grinding on the pozzolanic activity of residual sugarcane bagasse ash, Int. RILEM Conf. Use Recycl. Mater. Build. Struct. (2004) 731–740, https://doi.org/10.1617/2912143756.081.
[4] G.C. Cordeiro, R.D. Toledo Filho, L.M. Tavares, E.M.R. Fairbairn, Pozzolanic activity and filler effect of sugar cane bagasse ash in Portland cement and lime mortars, Cem. Concr. Compos. 30 (2008) 410–418, https://doi.org/10.1016/j.cemconcomp.2008.01.001.
[5] F.C.R. Almeida, A. Sales, J.P. Moretti, P.C.D. Mendes, Sugarcane bagasse ash sand (SBAS): Brazilian agroindustrial by-product for use in mortar, Constr. Build. Mater. 82 (2015) 31–38, https://doi.org/10.1016/j.conbuildmat.2015.02.039.
[6] J.P. Moretti, A. Sales, F.C.R. Almeida, M.A.M. Rezende, P.P. Gromboni, Joint use of construction waste (CW) and sugarcane bagasse ash sand (SBAS) in concrete, Constr. Build. Mater. 113 (2016) 317–323, https://doi.org/10.1016/j.conbuildmat.2016.03.062.
[7] J.P. Moretti, A. Sales, V.A. Quarcioni, D.C.B. Silva, M.C.B. Oliveira, N.S. Pinto, L.W. S.L. Ramos, Pore size distribution of mortars produced with agroindustrial waste, J. Clean. Prod. 187 (2018) 473–484, https://doi.org/10.1016/j.jclepro.2018.03.219.
[8] S.A. Zareei, F. Amerib, N. Bahrami, Microstructure, strength, and durability of eco-friendly concretes containing sugarcane bagasse ash, Constr. Build. Mater. 184 (2018) 258–268, https://doi.org/10.1016/j.conbuildmat.2018.06.153.
[9] A. Sales, S.A. Lima, Use of Brazilian sugarcane bagasse ash in concrete as sand replacement, Waste Manag. 30 (2010) 1114–1122, https://doi.org/10.1016/j.wasman.2010.01.026.
[10] V.A. Franco-Luján, M.A. Maldonado-García, J.M. Mendoza-Rangel, P. Montes-García, Chloride-induced reinforcing steel corrosion in ternary concretes containing fly ash and untreated sugarcane bagasse ash, Constr. Build. Mater. 198 (2019) 608–618, https://doi.org/10.1016/j.conbuildmat.2018.12.004.
[11] L. Rodier, E. Villar-Cociña, J.M. Ballesteros, H.S. Junior, Potential use of sugarcane bagasse and bamboo leaf ashes for elaboration of green cementitious materials, J. Clean. Prod. (2019), https://doi.org/10.1016/j.jclepro.2019.05.208.
[12] A. Rajasekar, K. Arunachalam, M. Kottaisamy, V. Saraswathy, Durability characteristics of ultra high strength concrete with treated sugarcane bagasse ash, Constr. Build. Mater. 171 (2018) 350–356, https://doi.org/10.1016/j.conbuildmat.2018.03.140.
[13] D.-H. Le, Y.-N. Sheen, M.-N.-T. Lam, Self-compacting concrete with sugarcane bagasse ash - ground blast furnace slag blended cement: Fresh properties, IOP Conf. Ser. Earth Environ. Sci. (2018), https://doi.org/10.1088/1755-1315/143/1/012019.
[14] M. Rossi, For Cement's Massive Carbon Footprint, Some Concrete Steps, (2019). https://undark.org/2019/11/13/cement-carbon-green-concrete/ (accessed March 31, 2020).
[15] S.A. Lima, A. Sales, F.A.R. Do Couto, J.P. Moretti, K.F. Portella, Concretos com cinza do bagaço da cana-de-açúcar: avaliação da durabilidade por meio de ensaios de carbonatação e abrasão, Ambient. Construído. 11 (2011) 201–212, https://doi.org/10.1590/S1678-86212011000200014.
[16] P.O. Modani, M.R. Vyawahare, Utilization of bagasse ash as a partial replacement of fine aggregate in concrete, Procedia Eng, in, 2013, pp. 25–29.
[17] E. Arif, M.W. Clark, N. Lake, Sugar cane bagasse ash from a high-efficiency co-generation boiler as filler in concrete, Constr. Build. Mater. 151 (2017) 692–703, https://doi.org/10.1016/j.conbuildmat.2017.06.136.
[18] J.P. Moretti, S. Nunes, A. Sales, Self-compacting concrete incorporating sugarcane bagasse ash, Constr. Build. Mater. 172 (2018) 635–649, https://doi.org/10.1016/j.conbuildmat.2018.03.277.
[19] M.F. Gromboni, A. Sales, M.d.A.M. Rezende, J.P. Moretti, P.G. Corradini, L. H. Mascaro, Impact of agro-industrial waste on steel corrosion susceptibility in media simulating concrete pore solutions, J. Clean. Prod. 284 (2021) 124697.
[20] National minerals information Center, Mineral Commodity Summaries, (2021). https://www.usgs.gov/centers/national-minerals-information-center/mineral-commodity-summaries (accessed January 12, 2022).
[21] J.P. Moretti, Incorporação de resíduo agroindustrial em matrizes cimentícias, Universidade Federal de São Carlos, 2018.
[22] S.A.L. Bessa, Utilização da cinza do bagaço da cana-de-açúcar como agregado miúdo em concretos para artefatos de infraestrutura urbana, Universidade Federal de São Carlos, 2011.
[23] Associação Brasileira de Normas Técnicas, NBR 15895 - Pozzolanic materials - Determination of fixed calcium hydroxide content - Modified Chapelle method, (2010).
[24] Associação Brasileira de Normas Técnicas, NBR 5751 - Pozzolanic materials - Determination of pozzolanic activity - Pozzolanic activity index with lime, (2019).
[25] Associação Brasileira de Normas Técnicas, NBR 12653 - Pozzolanic materials - requirements, (2015).
[26] ASTM International, E 323–11 - Standard Specification for Wire Cloth and Sieves for Testing Purposes 80 (2016) 2–6, https://doi.org/10.1520/E0323-11R16.2.
[27] ASTM International, G1-03 - Standard practice for preparing, cleaning, and evaluating corrosion test, (2017) 1–9. 10.1520/G0001-03R11.2.
[28] M. Rezende, P. Gromboni, P. Corradini, A. Sales, L. Mascaro, Evaluation of reinforcement corrosion in cementitious composites modified with water treatment sludge, J. Braz. Chem. Soc. (2023).
[29] ABNT, NBR 13276 - Argamassa para assentamento e revestimento de paredes e tetos - Determinação do índice de consistência (Mortars applied on walls and ceilings - Determination of the consistence index), (2016) 6. 01.080.10; 13.220.99.
[30] ABNT, NBR 9778 - Argamassa e concreto endurecidos - Determinação da absorção de água, índice de vazios e massa específica (Hardened mortar and concrete -

Determination of water absorption, voids and specific gravity), Assoc. Bras. Normas Técnicas. (2005) 8. 01.080.10; 13.220.99.
[31] D.V. Ribeiro, C.A.C. Souza, J.C.C. Abrantes, Use of electrochemical impedance spectroscopy (EIS) to monitoring the corrosion of reinforced concrete, Rev. Ibracon Estruturas e Mater. 8 (2015) 529–546, https://doi.org/10.1590/S1983-41952015000400007.
[32] P.H. Refait, M. Abdelmoula, J.-M.-R. Génin, Mechanisms of formation and structure of green rust one in aqueous corrosion of iron in the, Corros. Sci. 40 (1998) 1547–1560.
[33] S. Ghorbani, I. Taji, M. Tavakkolizadeh, A. Davodi, J. de Brito, Improving corrosion resistance of steel rebars in concrete with marble and granite waste dust as partial cement replacement, Constr. Build. Mater. 185 (2018) 110–119, https://doi.org/10.1016/j.conbuildmat.2018.07.066.
[34] C.Q. Ye, R.G. Hu, S.G. Dong, X.J. Zhang, R.Q. Hou, R.G. Du, C.J. Lin, J.S. Pan, EIS analysis on chloride-induced corrosion behavior of reinforcement steel in simulated carbonated concrete pore solutions, J. Electroanal. Chem. 688 (2012) 275–281, https://doi.org/10.1016/j.jelechem.2012.09.012.
[35] K. Scrivener, A. Ouzia, P. Juilland, A. Kunhi Mohamed, Advances in understanding cement hydration mechanisms, Cem. Concr. Res. 124 (2019), 105823, https://doi.org/10.1016/j.cemconres.2019.105823.
[36] P.K. Mehta, P.J.M. Monteiro, Concreto: microestrutura, propriedades e materiais, 4ª edição, Ibracon, São Paulo, 2014.
[37] ASTM International, C876 - 15 - Standard test method for corrosion potentials of uncoated reinforcing steel in concrete, (2015) 8. 10.1520/C0876-15.2.
[38] N.U. Amin, Use of bagasse ash in concrete and its impact on the strength and chloride resistivity, J. Mater. Civ. Eng. 23 (2011) 717–720, https://doi.org/10.1061/(ASCE)MT.1943-5533.0000227.